Cluster and DMSP observations of SAID electric fields

P A Puhl-Quinn, H Matsui, E Mishin, C Mouikis, L Kistler, Y Khotyaintsev,
Pierrette Décréau, E Lucek

HAL Id: insu-01408871

https://insu.hal.science/insu-01408871

Submitted on 5 Dec 2016

Cluster and DMSP observations of SAID electric fields

P. A. Puhl-Quinn,[1] H. Matsui,[1] E. Mishin,[2] C. Mouikis,[1] L. Kistler,[1] Y. Khotyaintsev,[3] P. M. E. Décréau,[4] and E. Lucek[5]

[1]   We report on magnetically conjugate Cluster and the Defense Meteorological Satellite Program (DMSP) satellite observations of subauroral ion drifts (SAID) during moderate geomagnetic activity levels on 8 April 2004. To our knowledge, the field-aligned separation of DMSP and Cluster ($\approx$28,000 km) is the largest separation ever analyzed with respect to the SAID phenomenon. Nonetheless, we show coherent, subauroral magnetosphere-ionosphere (MI) coupling along an entire field line in the post-dusk sector. The four Cluster satellites crossed SAID electric field channels with meridional magnitude E_M of 25 mV/m in situ and latitudinal extent $\Delta\Lambda \approx 0.5°$ in the southern and northern hemispheres near 07:00 and 07:30 UT, respectively. Cluster was near perigee ($R \approx 4\ R_E$) and within 5° (15°) of the magnetic equator for the southern (northern) crossing. The SAID were located near the plasmapause—within the ring current-plasmasphere overlap region. Downward field-aligned current signatures were observed across both SAID crossings. The most magnetically and temporally conjugate SAID field from DMSP F16A at 07:12 UT was practically identical in latitudinal size to that mapped from Cluster. Since the DMSP ion drift meter saturated at 3000 m/s (or $\sim$114 mV/m) and the electrostatically mapped value for E_M from Cluster exceeded 300 mV/m, a magnitude comparison of E_M was not possible. Although the conjugate measurements show similar large-scale SAID features, the differences in substructure highlight the physical and chemical diversity of the conjugate regions.

1.   Introduction

[2]   Polarization jets [*Galperin et al.*, 1974] or subauroral ion drifts (SAID) [*Spiro et al.*, 1979] are latitudinally narrow, enhanced streams of westward convection ($\langle V_{West}\rangle \gtrsim 1$ km/s) equatorward of the electron plasma sheet. They are driven by meridional electric fields intensified in a low-conductive nightside subauroral ionosphere conjugate to the ring current/plasmasphere overlap region (RCPO). SAID are considered a subset of the subauroral polarization streams (SAPS) that include plasma flow events with both broad and narrow extents in latitude [*Foster and Burke*, 2002]. Understanding the SAPS/SAID phenomenon is important for studies of how the structure, dynamics, and chemistry of the midlatitude ionosphere-thermosphere system are coupled to the structure and dynamics of the RCPO region. The coupling occurs via electric fields and currents. Energy is transferred from the magnetospheric RCPO region into the ionosphere and thermosphere, causing, in some cases, extreme, geomagnetic activity-related variability. The ability to understand and model this phenomenon requires both ionospheric and magnetospheric observations.

[3]   While SAPS/SAID characteristics are well documented at ionospheric altitudes [e.g., *Spiro et al.*, 1979; *Karlsson et al.*, 1998; *Foster and Vo*, 2002; *Figueiredo et al.*, 2004], investigations at higher altitudes are much more scarce. *Anderson et al.* [2001] found over 110 examples of SAID at altitudes $\sim$9000 km from the Akebono satellite. Several of them had ionospheric counterparts at altitudes $\sim$840 km from DMSP, which were nearly identical when electrostatically mapped to a common altitude. This indicated no significant field-aligned potential drops between 840 and 9000 km within the SAID channel.

[4]   The near-equatorial, magnetospheric characteristics of SAPS/SAID are even less documented. This is largely due to the relatively long magnetospheric satellite orbital period combined with the extreme variability of both plasmapause position and geomagnetic conditions. In other words, being "in the right place at the right time" is a rarely satisfied condition. *Maynard et al.* [1980] presented the only two examples of SAID found near the plasmapause at $L = 4$ in a cursory survey of 2 years worth of the ISEE-1 electric field data set. Other studies have focused more on SAPS rather than SAID observations: Measurements from the Active Magnetospheric Particle Tracer Explorers IRM satellite

---

[1]Space Science Center, University of New Hampshire, Durham, New Hampshire, USA.
[2]Institute for Scientific Research, Boston College, Chestnut Hill, Massachusetts, USA.
[3]Swedish Institute of Space Physics, Uppsala, Sweden.
[4]LPCE/CNRS, Université d'Orléans, Orléans, France.
[5]Blackett Laboratory, Imperial College, London, UK.
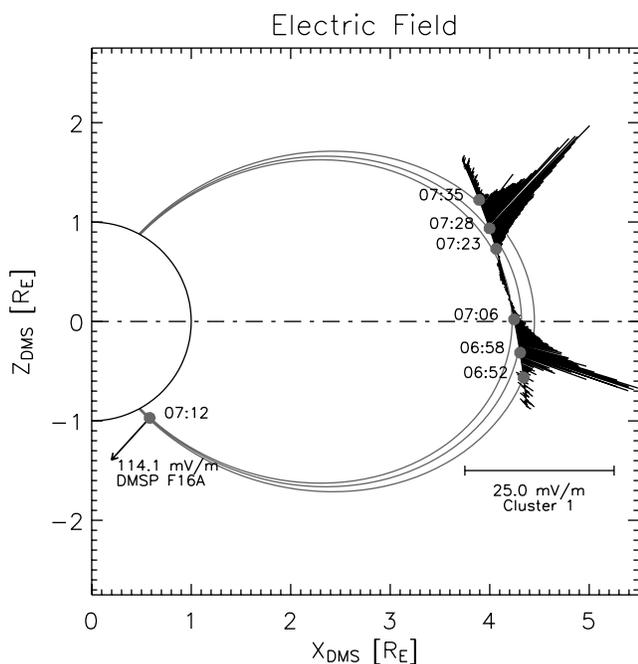
Electric Field

Figure 1. Cluster 1 and DMSP world-line plots showing the spatial locations of the SAID channels measured on 8 April 2004. Plotted are meridional electric field vectors. The coordinate $+Z_{DMS}$ is along magnetic north; the $X_{DMS}-Z_{DMS}$ plane is the meridional plane at MLT = 21:50 and $+Y_{DMS}$ points eastward. Dipolar field lines at $L = 4.225$, 4.30, and 4.45 are also plotted. Time tags (in UT) are indicated along the orbits.

showed the presence of enhanced irregular meridional (and outward) electric fields with $\langle E_Y \rangle \leq 3$ mV/m in RCPO near dusk [*LaBelle et al.*, 1988]. Mapped to the ionosphere, these fields would produce broad irregular SAPS with $\langle V_{West} \rangle \lesssim 1$ km/s; during the magnetic storm of 5 June 1991, the Combined Release and Radiation Effects Satellite observed several structured SAPS events in the RCPO alike those measured by DMSP in the topside ionosphere [*Burke et al.*, 2000; *Mishin and Burke*, 2005].

[5] In this paper we present near-equatorial magnetospheric and conjugate ionospheric observations of SAID electric fields from the Cluster and DMSP satellites, respectively. The polar Cluster orbit, with perigee at $\approx 4R_E$, allows the spacecraft to occasionally skirt along the L-shell-aligned plasmapause. During the inner-magnetospheric pass on 8 April 2004, a SAID channel was crossed both in the southern and northern hemisphere. Fortuitously, the DMSP F16A satellite was at about the same magnetic local time (MLT) and also measured a SAID event at a time in-between these crossings. The high degree of magnetic conjugacy between the electric fields from Cluster and DMSP allowed us for the first time to compare also other characteristics of the SAID event.

2. Instrumentation

[6] The four Cluster satellites [*Escoubet et al.*, 1997] fly in a tetrahedral formation of varying shape and size. Their center of mass executes an elliptical polar orbit with perigee

and apogee of ≈ 4 and 19 R_E, respectively. Each of the satellites carries an identical set of instrumentation. We present spin resolution (4 s) data from the following experiments: Electron Drift Instrument (EDI) measurements of DC electric field, **E** [*Paschmann et al.*, 1997]; Flux Gate Magnetometer (FGM) measurements of DC magnetic field, **B** [*Balogh et al.*, 2001]; Electric Fields and Waves Experiment (EFW) measurements of the spacecraft floating potential (U) and DC electric field [*Gustafsson et al.*, 1997]; Waves of High Frequency and Sounder for Probing Electron Density by Relaxation (WHISPER) experiment measurements of total electron density, N_e [*Décréau et al.*, 2001]; and Cluster Ion Spectrometry Experiment (CIS) measurements of proton differential energy flux [*Rème et al.*, 2001].

[7] The DMSP F16A satellite has a circular (~ 850 km altitude), sun-synchronous polar orbit near the 2000–0800 geographic meridian. The satellite carried a suite of sensors to measure (1) fluxes of precipitating electrons and ions in the energy range between 30 eV and 30 keV (SSJ5, [*Oberhardt et al.*, 1994]), (2) the ion and electron densities ($n_{i,e}$) and temperatures ($T_{i,e}$) and ion drift (SSIES, [*Rich and Hairston*, 1994]), and (3) perturbations of the Earth magnetic field (SSM).

3. Observations

[8] Quicklook auroral indices AU/AL and AE have been obtained through the Website of the WDC Kyoto for the time surrounding this event. One can clearly see a brief unmatched excursion in AL by ≤ -150 nT (and AE by ≥ 200 nT) at $\sim 06:10$ UT, indicating the development of DP 1 currents due to the onset of a substorm. There is another AL excursion (and AE increase) at about 07:00 UT. The sporadic and frequent nature of these onset signatures precludes the description of this time period as any specific storm phase.

[9] Figure 1 shows meridional electric field (E_M) vectors along the Cluster 1 orbit in the dipole meridian system (DMS), which is fixed with respect to magnetic north ($+Z_{DMS}$) and a particular value of MLT. The $X_{DMS}-Z_{DMS}$ plane is the meridional plane at 21:50 MLT, and $+Y_{DMS}$ points eastward. The Cluster orbit was within 5° of the 21:50-MLT meridional plane for the time range shown. The grey circles along the orbit, along with the associated time tags, denote crossing times into and out of the SAID channel, as well as the center crossing times of the channel (i.e., 06:58 and 07:28 UT). Cluster 2, 3, and 4 orbits are very similar. At this time, the four spacecrafts are flying with minimum and maximum separations of 300 and 1000 km, respectively. The grey lines are dipole field lines at $L = 4.225$, 4.30, and 4.45. The largest E_M values within the channel as measured by Cluster approach 25 mV/m in situ. The DMSP F16A observation of a SAID electric field at 07:12 UT in the Southern Hemisphere is also indicated. The scale for the vector representation of this field is different from that of the Cluster fields, with a maximum value of 114 mV/m. DMSP observed the SAID channel at 22:36 MLT, i.e., slightly underneath the $X_{DMS}-Z_{DMS}$ plane.

[10] Figure 2 shows the southern portion of the Cluster inner-magnetospheric pass of 8 April 2004. The northern portion of the pass (not shown) shows very similar features. The standard color coding for the Cluster mission is used,
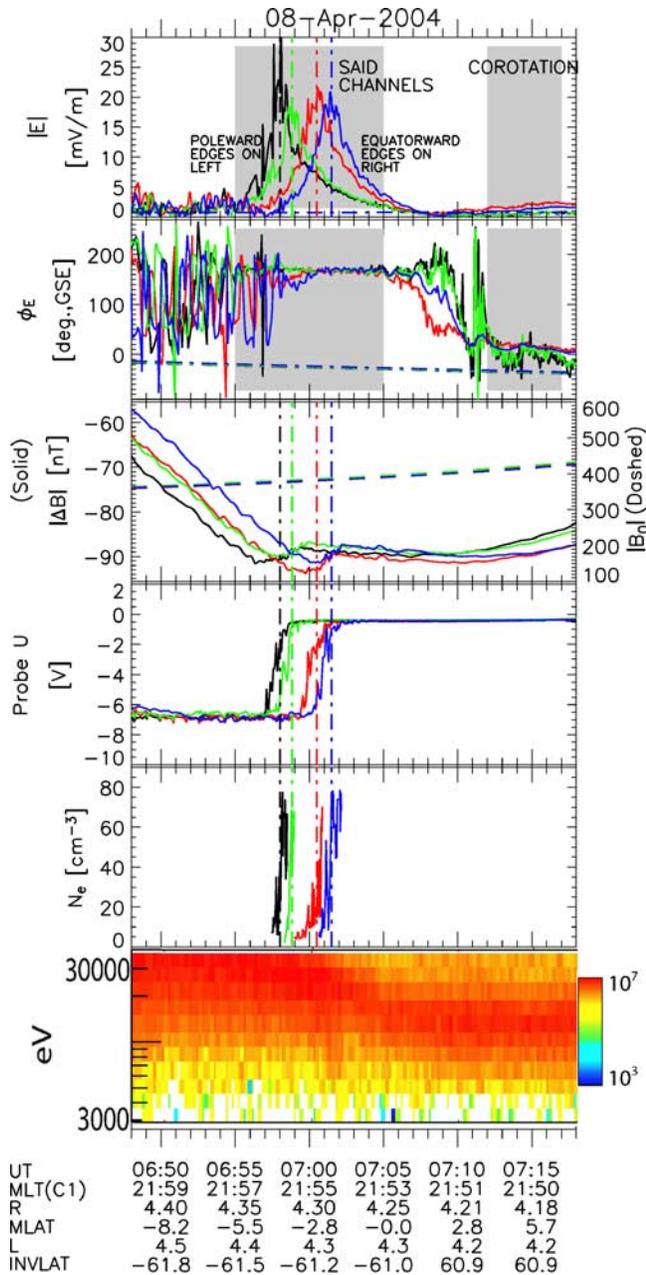
Figure 2. Cluster data on 8 April 2004 showing the southern portion of an inner-magnetospheric pass (ephemeris data for Cluster 1 is tabulated at the bottom). In the order from top to bottom are the electric field magnitude and the GSE azimuth angle (with the largely horizontal dash-dot lines showing corotation electric field values), the magnitude of the perturbation magnetic field $|\Delta\mathbf{B}| = |\mathbf{B}_{\mathrm{Cluster}} - \mathbf{B}_{\mathrm{IGRF}}|$ (with the dashed line being $\mathbf{B}_{\mathrm{IGRF}}$, and with its own scale on the right of the plot), the EFW probe potential, the electron density as derived from the WHISPER experiment, and the Cluster 4 energy-time spectrogram (in units of differential energy flux) from the CIS/CODIF experiment for H^+. Excluding the bottom panel, the colors black, red, green, and blue denote spacecrafts 1, 2, 3, and 4, respectively. The vertical dash-dot lines in panels 1, 3, 4, and 5 denote the SAID channel centers.

where Cluster 1, 2, 3, and 4 data are plotted in black, red, green, and blue, respectively. From top to bottom are the electric field magnitude and GSE azimuth angle (with the largely horizontal dash-dot lines showing corotation electric field values), the magnitude of the perturbation magnetic field $|\Delta\mathbf{B}| = |\mathbf{B}_{\mathrm{Cluster}} - \mathbf{B}_{\mathrm{IGRF}}|$ (where a negative sense is chosen to highlight the fact that the earth's field is being depressed, and with the dashed line being $|\mathbf{B}_{\mathrm{IGRF}}|$, and with its own scale to the right of the plot), the EFW probe potential, the electron density as derived from the WHISPER experiment, and the Cluster 4 omnidirectional energy-time spectrogram (in units of differential energy flux) from the CIS/CODIF experiment for H^+.

[11] The electric field traces (panels 1 and 2) for SC1 and SC3 (black and green) are from the EDI experiment while those for SC2 and SC4 (red and blue) are from the EFW experiment. The shaded regions highlight two electric field features: SAID and corotation (the largely horizontal dashed lines denote nominal corotation values). The vertical dash-dot lines denote the largest value of electric field magnitude (which is almost purely meridional in this case, with a value of ≈25 mV/m) at centers of the SAID channels. These lines extend into panels 3, 4, and 5 in order to highlight the SAID channel colocation with various field and plasma features.

[12] The magnetic field traces (panel 3) show a large-scale depression of the Earth's field ~25%, most likely due to a substantial ring current [cf., *Jorgensen et al.*, 2004; *Mishin and Burke*, 2005], and a smaller-scale current system coincident with the SAID channel near 07:00 UT. The smaller-scale system is discussed in detail below.

[13] Panels 4 and 5 show SAID colocation with sharp density gradients. Although the EFW probe potential, U, can often be used to derive the total electron density [*Laakso and Pedersen*, 1998], it is shown here to illustrate the overall coincidence and timing of the four plasmapause crossings with the four SAID channels. One of the main functions of the WHISPER experiment is the determination of total electron density in the range from 0.25 to 80 cm^{-3} [*Décréau et al.*, 2001]. Actual electron density values derived from the WHISPER experiment are shown in panel 5. The WHISPER passive spectra (2.2 s resolution) were used to estimate the total electron density. Values of the electron plasma frequency, F_{pe}, were manually identified as the low-frequency cutoff of natural emissions. F_{pe} is related to the total electron density by F_{pe} [kHz] $\sim$ sqrt(81 N_{e} [cm^{-3}]). We identify the overall sharp increase by a factor of 7 or so (from 10 cm^{-3} to more than 70 cm^{-3}) as the "knee" structure of the plasmapause. The temporal sequencing of the four knees mimics that of the peak electric field within the SAID channels (see panel 1). The smaller-scale density irregularities within the knee structure are real and supported by similar signatures in the interleaved active spectra and also by similar signatures in the density profile derived from the EFW spacecraft potential measurement.

[14] Panel 6 shows the Cluster 4 omnidirectional energy-time spectrogram from the CIS/CODIF experiment for H^+. The energy range is from 3 to 40 keV, and the units are differential energy flux. What is clear is that this ring current energy population coexists across the density gradient boundary (i.e., across 07:02 UT). In other words, the ring current population overlaps the cold, dense plasmaspheric
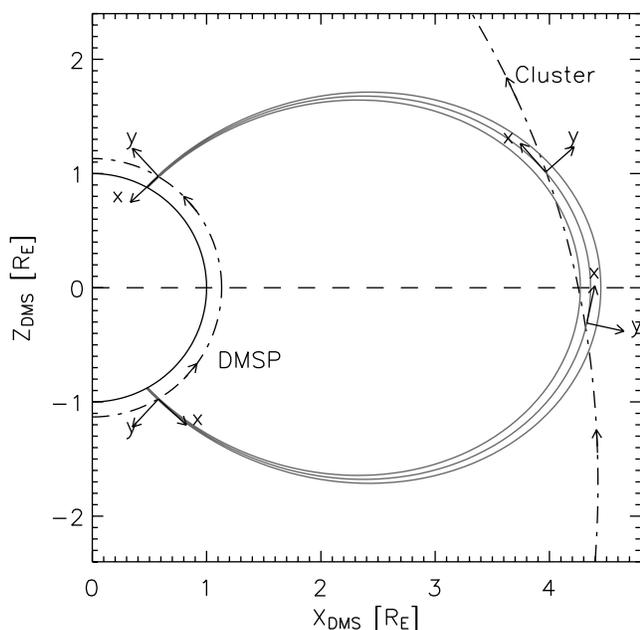
Figure 3. Coordinate systems used in this paper. The coordinate $+Z_{DMS}$ is along magnetic north; the $X_{DMS}-Z_{DMS}$ plane is the meridional plane at MLT = 21:50 and $+Y_{DMS}$ points eastward. Dipolar field lines at $L = 4.225$, 4.30, and 4.45 are also plotted. The local, magnetic-field-aligned (MFA) system (x, y, z) is defined for both ionospheric and magnetospheric observations such that x is B_0-aligned, y points across L-shell, and z points eastward. Note that y points poleward in both ionospheres and outward near the equator. The Cluster and DMSP orbital tracks are plotted as dash-dot lines.

population, confirming the coincidence of the SAID channel with the RCPO region. Across the plasmapause, the ion population experiences a slight energy shift, as well as pitch-angle reorganization (not shown). The time and spatial history of the population is quite crucial in order to understand these changes [*Kistler et al.*, 1989].

[15] We introduce at this time a local, magnetic-field-aligned (MFA) coordinate system (x, y, z), which is similarly defined for both magnetospheric and ionospheric observations. Figure 3 illustrates the relationship of (x, y, z) to the DMS system defined previously. The coordinate x is B_0-aligned, the y points across L-shell, and the z points eastward (note that B_0 is defined as the IGRF-90 model at DMSP. At Cluster, both the IGRF-90 model and the polynomial fitting to **B** were investigated as candidates for B_0, so the definition of B_0 at Cluster can be either of these two. In the subsequent analysis, it is made very clear which of the two is used to detrend the Cluster magnetic field and to define the MFA system). In the high-latitude northern (southern) ionosphere, (x, y, z) corresponds to [downward (upward), poleward, eastward]. Near the magnetic equator, the (x, y, z) corresponds to (northward, outward, eastward). Note that x and y are meridional, and z is always eastward. The Cluster and DMSP orbital tracks are plotted as dash-dot lines. Unless otherwise indicated, subsequent reference to (x, y, z) coordinates in this paper are with respect to this MFA system.

[16] The investigation of the SAID field-aligned current (FAC) system at both DMSP and Cluster was undertaken.

The goal of the SAID FAC investigation is to first isolate the SAID current structure at both DMSP and Cluster and then to compare the magnitude and spatial profile across the SAID channel between DMSP and Cluster. Isolating the FAC structure at DMSP was done using the standard method of subtracting off the IGRF field and looking for gradients in azimuthal (east-west) magnetic perturbations as the satellite travels across L-shell (the results of this calculation at DMSP are described in the paragraph relating to Figure 5). Applying this same method at Cluster (i.e., using IGRF to detrend the magnetic field) is deemed inappropriate since the detrended field could contain contributions from large-scale current systems and, thus, could mask those field variations responsible for the SAID FAC. In other words, the main issue regarding the calculation of SAID FAC at Cluster is the subtraction of the "most appropriate" background magnetic field which will isolate those magnetic perturbations caused by the SAID FAC. We feel that the most appropriate subtraction would be one which confines the largest magnetic perturbation field gradients to the region within and surrounding the SAID channel. There should be no large-scale trends in the magnetic perturbation field. For a polynomial fit, the fitting window should be large enough to capture the large-scale trends of interest in the immediate region but should be small enough so as not to be responsible for large-scale systems in adjacent regions.

[17] The large-scale currents of interest in this region have been shown to exist in all three directions of a cylindrical magnetic coordinate system: azimuthal, radial, and field-aligned [e.g., *Iijima et al.*, 1990; *Vallat et al.*, 2005]. Furthermore, in particular, for Cluster's orbit at 22 MLT on this day in April 2004, it is most likely embedded in radially inward, azimuthally westward, and downward field-aligned currents according to the statistical results of the aforementioned studies. From Ampere's law, we know that the gradients in the east-west magnetic perturbation field can be a result of either radial or field-aligned currents depending on the spatial profile. They cannot be a result of an azimuthal ring current. So the possible advantage of the polynomial fit versus the IGRF field as a detrending field would be to remove the trend caused by radial currents. Also, regarding the current systems in this region, we are not trying to exclude the Region 2 current system since the standard explanation of SAID/SAPS is that the Region 2 FACs' closure in the low-conductance ionosphere results in large E-fields. So these current systems, Region 2 and SAID FAC, are intimately linked and, perhaps, the same entity.

[18] To address the large-scale currents at Cluster, we first tried applying the multispacecraft curlometer technique. Note that this was already assumed not to be an option for the SAID FAC system because not all of the spacecrafts are in the current sheet at the same time. However, for the larger-scale system, we thought that it might work. As mentioned above, this has been performed successfully in the inner magnetosphere using Cluster data by *Vallat et al.* [2005]. Unfortunately, as predicted by *Vallat et al.* [2005], the Cluster tetrahedron shape, size, and orientation relative to the background magnetic field prevent the successful application of this technique. Specifically, the "dipole field truncation error contribution" is very large.
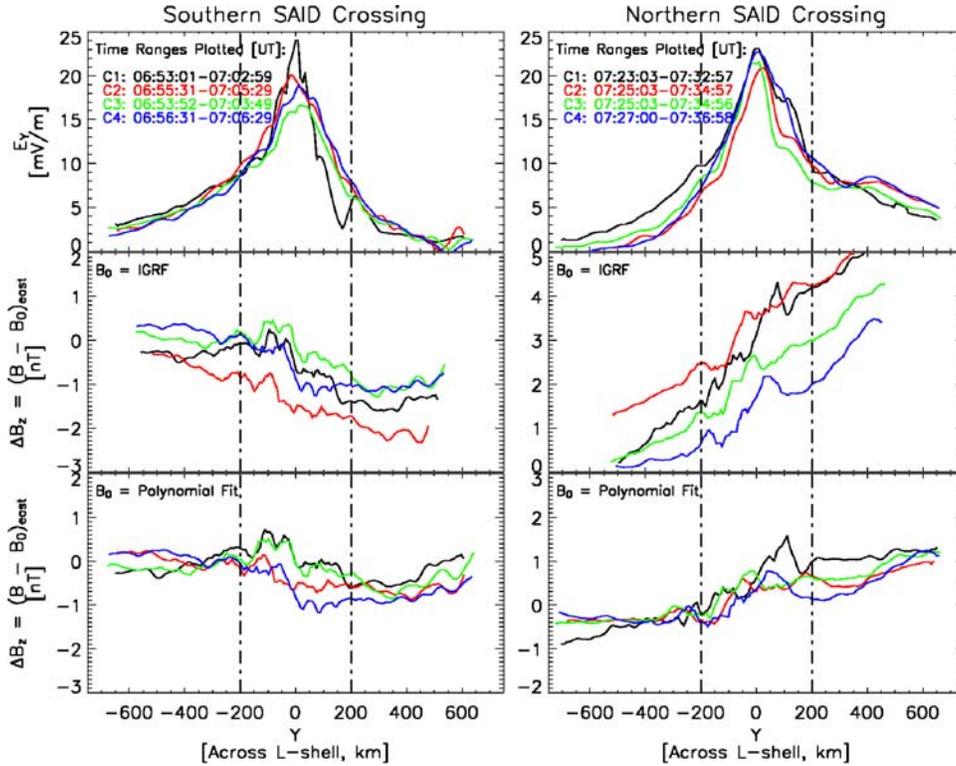
Figure 4. SAID FAC system measured by Cluster. The left panels are for the southern SAID crossing, and the right panels are for the northern crossing. All quantities are plotted as a function of distance, *Y*, across L-shell. The distance, *Y*, is measured with respect to the center E_M peak of the SAID channel. The top panel shows the meridional (across L-shell) component of the electric field. The middle panel shows azimuthal perturbation magnetic field, ΔB_Z, using the IGRF as the background (detrending) field, $\mathbf{B}_0$. The bottom panel shows ΔB_Z using a polynomial fit for $\mathbf{B}_0$. The vertical dash-dot lines denote the approximate width of the channel. The negative (positive) slope of ΔB_Z in the left (right) panels indicates field-aligned current into the southern (northern) ionosphere, a direction consistent with the Region 2 current system for the post-dusk sector. The colors black, red, green, and blue denote spacecrafts 1, 2, 3, and 4, respectively.

[19] We then investigated detrending of the magnetic field at Cluster using polynomial fitting, with fit windows centered on each SAID crossing and with widths ranging from 20 to 80 min. The optimal window, which reduced large-scale trends in the magnetic perturbation field, was 40 min. Using windows larger than this left large-scale trends in $\Delta\mathbf{B}$. Figure 4 shows Cluster measurements of the SAID field-aligned current (FAC) structure coincident with both southern and northern SAID channel crossings. The left panels are for the southern SAID crossing, whereas the right panels are for the northern crossing. All quantities are plotted as a function of distance, *Y*, across L-shell. The distance, *Y*, is measured with respect to the center E_M peak of the SAID channel. The top panel shows the meridional (across L-shell) component of the electric field. The middle panel shows the azimuthal perturbation magnetic field, ΔB_Z, using the IGRF as the detrending field, $\mathbf{B}_0$. The bottom panel shows the ΔB_Z using a polynomial fit for $\mathbf{B}_0$. The vertical dash-dot lines denote the approximate width of the channel. The negative (positive) slope of ΔB_Z in the left (right) panels indicates field-aligned current into the southern (northern) ionosphere, a direction consistent with the Region 2 current system for the post-dusk sector. The colors black, red, green, and blue denote spacecrafts 1,

2, 3, and 4, respectively. It shows that using a polynomial fit for detrending indeed reduced the large-scale trend, especially in the Northern Hemisphere. The gradient within the SAID channel was also reduced by a factor of approximately 3 for the northern crossing. For the southern crossing, the gradients remain largely unchanged. However, we note that the infinite current sheet approximation for the southern crossing is not a very good one, as there are gradients in the radial magnetic perturbation which are on the order of the east-west perturbations. This can be understood by the fact that the southern crossing occurs only 4° from the magnetic equator, so that the FAC signal might not be strong enough to be measured. We are still seeing a sheet-like structure in the Northern Hemisphere (at 14° from the equator), but the southern crossing of SAID is too close to the equator.

[20] As mentioned, the thin current sheet approximation, where $\mu_0 j_\parallel = \frac{\partial(\Delta B_z)}{\partial Y}$, can be applied at the northern crossing. We consider the detrended signal using IGRF as providing an upper limit to the gradient, and we regarded the detrended signal using the polynomial fit as providing a lower limit. An initial estimate of the variation of ΔB_Z is in the range from 1.0 to 3.0 nT gain over 400 km, yielding a "downward" $j_\parallel$, or, $j_\parallel^i = 2.0 - 6.0 \frac{nA}{m^2}$ in situ. Magnetic lensing of $j_\parallel^i$ to DMSP altitude, i.e., assuming $\nabla \cdot \mathbf{j} = 0$ and $\mathbf{j}_\perp = 0$
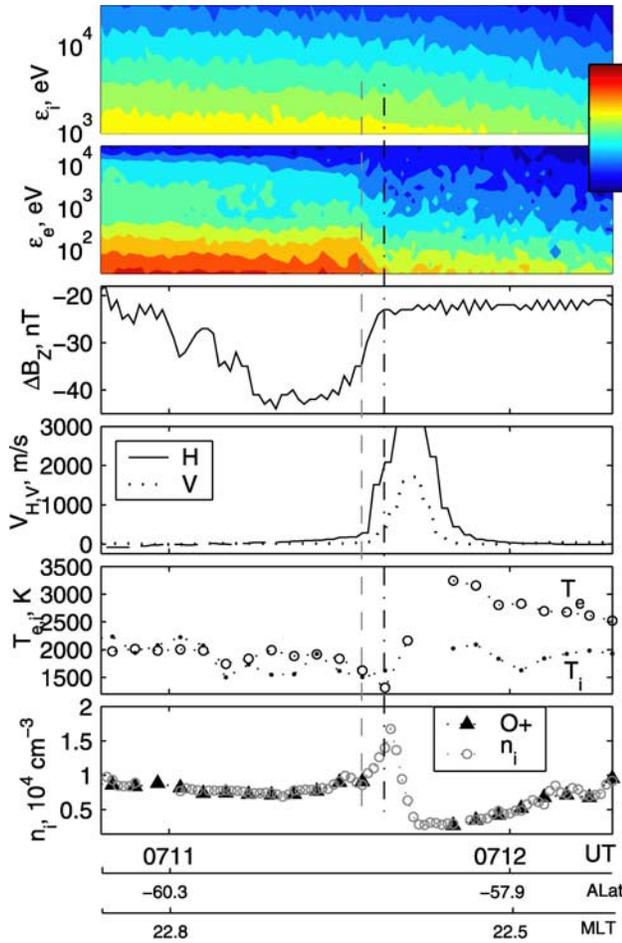
Figure 5. A SAID event observed by F16A: Downcoming ion and electron directional differential number fluxes in $cm^{-2}\ s^{-1}\ ster^{-1}\ eV^{-1}$ (top panels); ΔB_Z (panel 3); vertical and horizontal components of the ion drift velocity (panel 4); the electron and ion temperatures (panel 5); the plasma density (bottom). Vertical dash-dotted and dashed lines encompass the SAID's poleward edge.

along a flux tube connecting Cluster ($B_0 \approx 440$ nT at the northern crossing) to DMSP altitude ($B_0 \approx 38{,}000$ nT), yields $j_{\parallel}^{\downarrow} = 0.17$–$0.50\ \frac{\mu A}{m^2}$. This is a very rough estimate, of course, but we feel that we have successfully isolated the SAID FAC at least in the Northern Hemisphere, identified it as downward, and approximated an appropriate range for its value. Although wave analysis is beyond the scope of this paper, it is interesting to note the onset of magnetic perturbations within the SAID channel. SAPS wave structures (SAPSWS) are an important component of subauroral MI coupling [e.g., *Mishin et al.*, 2003; *Mishin et al.*, 2004]. This analysis will be part of a future effort.

[21] Figure 5 shows the data from DMSP F16A. From top to bottom are the spectrograms of precipitating ions and electrons, the azimuthal perturbation magnetic field, ΔB_Z, the horizontal (H) and vertical (V) ion drift velocities, the electron and ion temperatures, and the total (n_i) and O^+ ion densities. The magnetic field data are presented as a difference ($\Delta \mathbf{B}$) between the measured values and the IGRF-90 model ($\mathbf{B_0}$). The SAID feature of interest is a narrow spike, $\Delta\Lambda \lesssim 0.6°$, in the sunward velocity at $\sim 07{:}11{:}(35$–$49)$ UT,

~ 22.6 MLT, and $\sim -59.1\ A_{Lat}$ (the apex latitude ALAT $\approx$ ILAT). The V_H and the corresponding poleward electric field exceeded the drift meter's upper limit of 3 km/s and ~ 114 mV/m, respectively. The poleward (outer) edge of the SAID channel is indicated by the vertical dashed line at 07:11: 34 UT. It is colocated with the onset of a dispersion-less decrease in fluxes of energetic electrons and sharp increase in ΔB_Z and n_i. The ΔB_Z growth ended at 07:11:38 UT (the dash-dotted line). Given a satellite's speed of 7.5 km/s, an ≈ 12-nT gain corresponds to downward Region 2 field-aligned current (R2 FAC) $j_{\parallel}^{\downarrow} \approx 0.32\ \frac{\mu A}{m^2}$. By the same token, upward Region 1 FAC of $j_{\parallel}^{\uparrow} \approx 0.1$–$0.2\ \frac{\mu A}{m^2}$ flows at high latitudes. Note that (1) the SAID's core was equatorward of the R2 FAC, (2) the plasma density fell within the SAID's core, and (3) the density trough extended to the equator of the SAID channel and its depth decreased in step with T_e [cf. *Mishin et al.*, 2004]. Unlike the other features, the precipitating ion population has not shown any significant variation across the SAID channel.

[22] Note that DMSP F13, F14, and F15 observed SAID events which were practically identical to that of F16A. Table 2 summarizes the SAID FAC values obtained for F14, F13, F16A, Cluster (northern only), and F15. Table 1 summarizes the temporal and spatial characteristics of the 12 SAID observations (8 from Cluster and 4 from DMSP). From left to right, we have spacecraft ID (F13, F14, F15, and F16A denoting DMSP fleet, and C1, C2, C3, and C4 denoting the Cluster spacecraft), SAID center time—in UT (the table is ordered by this time), hemisphere ("S"outhern or "N"orthern), magnetic local time (MLT), magnetic latitude (MLAT), radius (R), and invariant latitude (ILAT$_T$, based on the magnetic field model of *Tsyganenko* [2002a, 2002b], rather than a dipole field).

4. Discussion
4.1. The 12 Multispacecraft SAID Crossings: Temporal and Spatial Characteristics

[23] The 12 SAID observations listed in Table 1 allow estimates to be made regarding temporal and spatial characteristics. Temporally, SAID onset around 06:18 UT occurs within 10 min of the substorm onset at 06:10 UT. Observation of the SAID channel persists until 07:53:00, giving it a duration of at least 1.5 hours. The time delay of ~ 10 min is consistent with the substorm injection mechanism which involves dipolarization electromagnetic pulses that propagate earthward and expand azimuthally with speeds of tens

Table 1. SAID Channel Ephemeris Parameters

SC ID	UT on 8-Apr-2004	H	MLT	MLAT, [Deg]	R, [R_E]	ILAT$_T$, [Deg]
F14	06:18:00	S	21:48	−59.14	1.13	−61.0
F13	06:46:00	S	20:22	−56.9	1.13	−59.0
C1	06:58:00	S	21:56	−4.15	4.32	−58.4
C3	06:58:50	S	21:56	−4.49	4.31	−58.4
C2	07:00:30	S	21:56	−3.87	4.32	−58.4
C4	07:01:30	S	21:57	−4.73	4.31	−58.4
F16A	07:11:45	S	22:36	−56.30	1.13	−58.4
C1	07:28:00	N	21:44	13.18	4.11	60.5
C2	07:30:00	N	21:44	13.49	4.10	60.5
C3	07:30:00	N	21:44	13.56	4.09	60.5
C4	07:32:00	N	21:44	13.29	4.08	60.5
F15	07:53:00	S	23:14	−56.10	1.13	−58.2
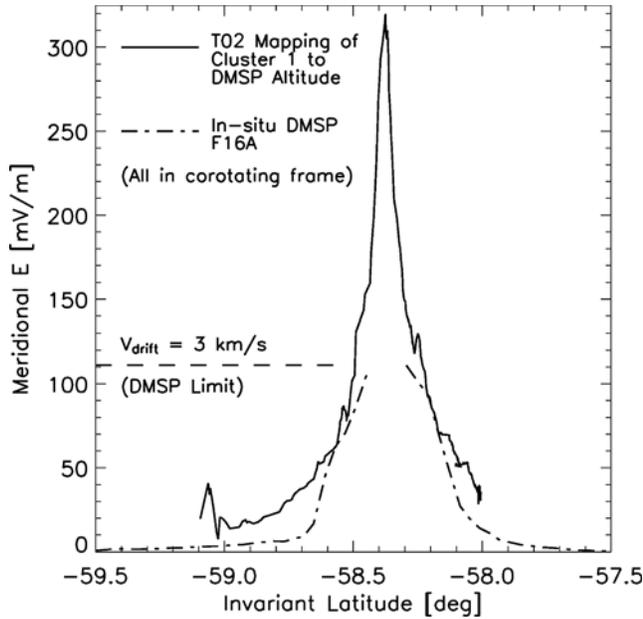
Figure 6. Mapping of Cluster 1 electric field to DMSP altitude (solid line) and in situ DMSP F16A electric field (dash-dot line) as functions of invariant latitude. The horizontal dashed line at 114 mV/m (corresponding to 3 km/s) indicates the instrumental limit of the F16A drift meter.

of kilometers per second [e.g., *Thomsen et al.*, 2001]. Furthermore, the dispersionless cutoff of electron fluxes at the plasmapause, as opposed to the energetic ions, seems to indicate that the cold plasma density affects transport of the substorm-injected electrons. Spatially, the SAID center has an average invariant latitude of $\approx -59 \pm 1°$ (60.5°) in the Southern (Northern) Hemisphere. Azimuthally, the measurements collectively span 3 hours (45°) in MLT, with an average location of 21:53 MLT. These observations indicate that $\varepsilon_{\perp}$ 10-keV electrons have reached $L \sim 4$ and ~ 22 MLT within ~ 10 min after the substorm onset and remained there for at least 1 hour. These are useful observational parameters for SAPS/SAID electric field modelling efforts in the inner magnetosphere [e.g. *Goldstein et al.*, 2005a].

4.2. Electric Field and Field-Aligned Current: Large-Scale MI Coupling

[24] The highest degree of magnetic and temporal conjugacy was between DMSP F16A and Cluster 1 in the Southern Hemisphere. Temporally, the SAID observations were within 12 min of each other (07:00 UT for Cluster versus 07:12 UT for DMSP). Spatially, both DMSP and Cluster were at $\approx -58.4°$ invariant latitude and within 10° MLT of each other (21:56 MLT for Cluster versus 22:36 MLT for DMSP). They were separated by a field-aligned distance of $\approx 28,000$ km (4.4 R_E). To our knowledge, this is the largest field-aligned separation ever analyzed with respect to the SAID phenomenon. Since subauroral magnetosphere-ionosphere (MI) coupling occurs via electric fields and electrical currents, the following discussion focuses on these two parameters of the conjugate system.

[25] Electrostatic direct mapping along magnetic field lines breaks down when parallel electric fields and/or time dependence is present, which is often the case at auroral

latitudes during the growth phase of substorms [*Toivanen et al.*, 1998]. In our case, we deal with subauroral latitudes and a time that, while geomagnetically active, was well removed from any well-defined substorm growth or recovery phases. Figure 6 shows the electrostatic mapping of the Cluster 1 electric field to DMSP altitude (solid line) and the in situ DMSP F16A electric field (dash-dot line) as functions of invariant latitude. For the mapping, we used the model of *Tsyganenko* [2002a, 2002b], which shows better agreement with in situ Cluster magnetic field measurements than IGRF-10 does. Inputs for the model include IMF and solar wind data from ACE and the SYM-H index. It is clear that the degree of conjugacy with respect to invariant latitude is quite high, with the two structures centered at $\sim -58.4°$. Also, the widths at the bases of the SAID structures agree on a value of $\approx 0.5°$. This is a typical, narrow latitudinal width for SAID structures. The peak magnitude of ≥ 300 mV/m on Cluster is not matched by F16A due to instrumental limitation. The F16A curve is truncated at the instrumental limit of the drift meter of ≈ 114 mV/m (the dashed horizontal line). However, it is clear from the shape of the F16A curve that the electric field peak would have exceeded this limit. That F16A would have measured 300 mV/m, however, cannot necessarily be assumed. *Weimer et al.* [1985] showed with conjugate DE1 and DE2 electric field data that small-scale current closure might occur at altitudes higher than that of F16A (i.e., higher than 850 km). Indeed, *Smiddy et al.* [1977] observed 280 mV/m at an altitude of 1463 km.

[26] Field-aligned current in an MI coupling system can be simply related to both electric and magnetic field variations. Since our observations indicate a temporal stability on the order of hours, we model the SAID channel as a static structure. Ionospheric current continuity ($\nabla \cdot \mathbf{j} = 0$), combined with the height-integrated ionospheric Ohm's law and assuming that no parallel current flows out the bottom of the ionosphere, yields $j_{\parallel}^{\text{top}} = \pm \nabla_{\perp} \cdot (\Sigma_P \mathbf{E}_{\perp} - \Sigma_H \mathbf{E}_{\perp} \times \hat{b})$ for the parallel current entering (or exiting) the topside ionosphere. The plus (minus) sign refers to the Northern (Southern) Hemisphere, respectively, and Σ_P (Σ_H) is the height-integrated Pedersen (Hall) conductivity. Field-aligned current is also related to magnetic variations via Ampere's law: $j_{\parallel} = \frac{1}{\mu_0} (\nabla \times \Delta \mathbf{B})_{\parallel}$, where $\Delta \mathbf{B}$ is the perturbation magnetic field assumed to be responsible for $j_{\parallel}$. Using the (x, y, z) system shown in Figure 3, and assuming a poleward-directed electric field ($\mathbf{E}_{\perp} = E_y \hat{y}$), and spatial variation of the fields mostly in the $\hat{y}$ direction (latitudinally thin, longitudinally wide, L-shell-aligned channel), the two expressions for $j_{\parallel}$ combine to yield

$$\frac{1}{\mu_0} \frac{\partial(\Delta B_z)}{\partial y} = -\frac{\partial}{\partial y}\left(\Sigma_p E_y\right) \tag{1}$$

for the southern ionosphere (i.e., where DMSP F16A made its measurements).

[27] In this static case, continuity of electrical current requires that the horizontal (across L-shell) gradient of the azimuthal perturbation magnetic field in the topside ionosphere be balanced by the horizontal gradient of the product of the poleward electric field and the Pedersen conductivity. In the absence of horizontal conductivity gradients (i.e., assuming Σ_P is not a function of y), the electric field

Table 2. SAID FAC Observed by Cluster and DMSP on 8-Apr-2004

SC ID	UT on 8-Apr-2004	H	$j_\parallel^\perp \frac{nA}{m^2}$ (In Situ)	$j_\parallel^\perp \frac{\mu A}{m^2}$ (Lensed to DMSP Altitude)
DMSP F14	06:18	S	400	0.40
DMSP F13	06:46	S	212−282	0.21−0.28
DMSP F16A	07:12	S	320	0.32
Cluster	07:30	N	2.0−6.0	0.17−0.50
DMSP F15	07:53	S	100	0.10

gradients at the edges of the SAID channel would be solely supported by a pair of oppositely directed field-aligned current sheets, directed downward into the ionosphere on the equatorward edge and upward out of the ionosphere at the poleward edge. A quick estimate of the magnetic gradients required to sustain such a current configuration, assuming $\Sigma_P = 0.3$ S (after the work of *Smiddy et al.*, 1977), reveals that the F16A DMSP observations in the Southern Hemisphere (as shown in Figure 5) are wholly inconsistent with this picture: the 61-mV/m gain in E_y over 30 km on the poleward edge would require a 23-nT drop in ΔB_z; the 55-mV/m drop in E_y over 30 km on the equatorward edge would require a 21-nT gain in ΔB_z. What is observed in ΔB_z is a 12-nT gain on the poleward edge, and there is no significant variation at all on the equatorward edge. This implies the existence of strong horizontal conductivity gradients. It is known that the strength and morphology of the SAID $j_\parallel$ structure is quite variable. Initially, an FAC pair as described above is thought to develop as the channel is created. Over time, as the MI feedback process develops, and the ionospheric conductivity is modified and presumably the gradients develop, this paired FAC structure is no longer required to maintain the electric field channel. DMSP and Cluster are observing the channel at this later stage. While this reduction of conductivity is indicative of a constant current generator, *Figueiredo et al.* [2004] have concluded through the analysis of Astrid-2 satellite data that the SAID generation mechanism is neither a pure voltage nor a pure current generator. Their analysis shows that SAID have characteristics attributable to both types of generators.

[28] The azimuthal magnetic perturbations at both DMSP and Cluster SAID crossings are indicating downward FAC (see Figures 4 and 5 and Table 2). Substorm-related, subauroral, "Region 2" field-aligned current (R2 FAC) forms at locations of strong, azimuthal, hot ion pressure gradients which bound the crescent-shaped partial ring current [e.g., *Vasyliunas*, 1970]. Although the global morphology of R2 FAC is quite variable, and strongly depends on geomagnetic storm phase [e.g., *Liemohn et al.*, 2001], R2 FAC flows downward into both ionospheres when the pressure increases with local time (usually in the post-dusk sector) and upward out of the ionospheres when the pressure decreases with local time (usually in the postmidnight sector). This R2 FAC pattern has been shown statistically for disturbed geomagnetic conditions by *Iijima and Potemra* [1976]. The closure of downward R2 FAC with upward currents at higher latitudes via a northward Pederson current through the ionosphere can lead to SAID formation, especially in the substorm recovery phase [e.g., *Anderson et al.*, 1993; *Karlsson et al.*, 1998]. The specifics of SAID generation mechanisms will not be discussed here.

Suffice it to say that the strength of R2 FAC within SAID is time dependent due to the feedback process coupling ionospheric conductivity reduction and electric field growth, which are required to maintain current continuity. SAID have therefore been observed with varying ratios between electric field strength and R2 FAC strength [e.g., *Rich et al.*, 1980; *Anderson et al.*, 1991, 1993]. Ionospheric observations of SAID FAC range anywhere from 0 to 7 $\frac{\mu A}{m^2}$ [*Rich et al.*, 1980; *Anderson et al.*, 1993; *Anderson et al.*, 2001; *Figueiredo et al.*, 2004].

[29] As for the magnitudes of the SAID FAC estimates, magnetically lensing the Cluster value (in the Northern Hemisphere) to DMSP altitude results in rough agreement with F16A, F13, and F14 (again, see Table 2). However, the DMSP measurements are all taken in the Southern Hemisphere, whereas the Cluster measurements are in the north. If we can assume that DMSP would have measured similar FAC magnitudes in the north, the rough agreement between Cluster and DMSP could be suggesting that perpendicular current at and between the conjugate SAID observation sites is minimal (since our lensing assumption requires that $j_\perp = 0$ along the flux tube). In other words, the northern Cluster SAID crossing lies above any significant current conversion (perpendicular ↔ parallel) region. This notion is supported by the work of *Vallat et al.* [2005], who showed that for a similar pass, as Cluster climbs away from the magnetic equator and to higher latitude, the field-aligned current becomes stronger. The fact that the SAID FAC signal could not be "cleanly" determined at the southern Cluster SAID crossing, which is only 4° from the magnetic equator, and therefore might have a much weaker FAC signal fits into this picture as well.

4.3. Smaller-Scale SAID Channel Substructure

[30] We discuss the substructure of the SAID layer in terms of density profiles across the layer. In the ionosphere (see Figure 5), there are two distinct features of the density profile: the trough on the equatorward side of the channel and the plasmapause on the poleward side (i.e., between the two vertical lines in the density panel). In the magnetosphere (see Figure 2), the existence of a trough is not indicated. The density irregularities at Cluster are of a much smaller scale than expected for the projection of the ionospheric trough. The small-scale structures in density correlate with small-scale structures in the electric field (see panel 1 of Figure 2). Although dusk sector (and possibly SAID-related) troughs in the outer plasmasphere have been measured and modelled [e.g., *Horwitz et al.*, 1990 and *Ober et al.*, 1997, respectively], we find no evidence for a magnetospheric trough in our case. This supports the idea that the ionospheric density trough, which maps well inside the plasmasphere, is most likely caused by local ionospheric processes such as the ion outflow ($V_V \sim 2$ km/s) and enhanced ion-electron recombination due to strong electric fields and vibrational excitation of thermospheric molecules by thermal electrons [e.g., *Anderson et al.*, 1993; *Mishin et al.*, 2004].

[31] The relative location of the plasmapause (PP) to the SAID channel (i.e., whether the SAID channel lies "outside" or "inside" the PP) can give information on what type of streamlines (i.e., "open" or "closed") threads the channel. If "open", the SAID field could participate in the "stripping away" of, for instance, plasmaspheric bulges

(e.g., as shown by *Goldstein et al.*, 2005b). If "closed", it would just redistribute the thermal plasma in longitude. Observationally, the issue is complicated by the fact that the PP is not necessarily the convection boundary (CB) between open and closed streamlines but could, rather, be at a recent location of the CB. The studies of *Yeh et al.* [1991] and *Galperin et al.* [1997] are particularly relevant to our study because they focused on the implications of the relative latitudinal positions of the equatorward boundary of soft electron precipitation (SEB), the equatorward edge of the high-latitude, large-scale convection zone (CB), the plasmapause (PP), and the SAID channel. They show that the SEB is colocated with the CB during steady, moderately active and strong, prolonged storm-like conditions. In other words, the SEB denotes the equatorward extent of the low-energy $E \times B$ drift-dominated plasma sheet population. This implies that the injected low-energy electrons within the large-scale convection zone have not had time to be fully exhausted by precipitation. The SEB, as a convection boundary, has been further identified as an electron Alfvén boundary which can exhibit energy dispersion. Indeed, the empirical models of *Galperin et al.* [1974] and *Valchuck et al.* [1986] show that the invariant latitude of the 1- to 2-keV SEB lies $1-2°$ higher than the 100-eV SEB. One would expect a natural relationship between the SEB and the PP since the particle population of interest is relatively cold. The SEB is not, however, always colocated with the large, radial density drops of the PP. This is because of a delayed response of the density profile to changes in activity level. The PP, therefore, occurs at either the present CB (SEB) or at a recent location of the CB. Refilling rates determine the exact density profile. In relation to SAID, the SEB has been shown to lie at the poleward edge of the channel, i.e., in-between the high-latitude convection cell, and the lower-latitude SAID channel. This implies that the large-scale convection streamlines carrying plasma sheet electrons do no enter the SAID channel. The SAID are decoupled from their high-latitude convection counterpart. The equatorward precipitating ion boundary, however, has been shown to lie on the equatorward side of the SAID channel. The energetic electron and ion populations, therefore, are separated across the SAID channel.

[32] For our case, as indicated above, the ionospheric observations place the plasmapause on the poleward edge; that is, the SAID lies "inside" the plasmapause. Additionally, DMSP observes a dispersionless cutoff of $(30-10 \text{ keV})$ electron precipitation colocated with the PP, whereas the precipitating ion population shows no significant change across the channel. These observations are consistent with the Galperin/Yeh studies except that the dispersionless nature of the cutoff excludes the usual Alfvén layer interpretation. The fast (within 10 min) appearance of the SAID channel suggests that the PP position has not changed and that the dispersionless cutoff occurred at the preexisting PP. This implies a strong influence of the cold plasma density on the propagation of the dipolarization pulse, consistent with the modeling of the substorm injection events [e.g., *Birn et al.*, 1997; *Li et al.*, 1998], which usually assumes that the pulse is reflected and weakened at the PP. At Cluster, a close examination of the density reveals that the PP extends across the entire SAID channel so that classification of the channel as "outside" or "inside" is more difficult. Identifying the

precipitating populations at Cluster is also difficult due to the angular resolution of the particle instruments. More observations are needed in order to say whether the density profile at Cluster, in relation to the SAID channel, can add to the above discussion of streamline topology.

5. Conclusions

[33] We have presented multispacecraft (Cluster and DMSP) observations of a strong SAID event on 8 April 2004. Taken as an ensemble of 12 separate SAID crossings, the observations show a temporal stability of at least 1.5 hours, a center location at $58°$ ILAT and 21:53 MLT, and an azimuthal extent of $45°$. The highest degree of magnetic and temporal conjugacy was between DMSP F16A and Cluster in the Southern Hemisphere ($\Delta UT = 12$ min., $\Delta ILAT \sim 0°$, $\Delta MLT \sim 10°$). They were separated by a field-aligned distance of $\approx 28,000$ km (4.4 R_E). To our knowledge, this is the largest separation ever analyzed with respect to the SAID phenomenon. Large-scale features found to be common to both the ionospheric and magnetospheric data sets include a latitudinal width of $0.5°$ and an ionospheric downward FAC strength of $\sim 0.32 \frac{\mu A}{m^2}$. Comparison of the E_M peak magnitude was not possible due to the saturation of the ion drift meter. Smaller-scale features differ between the two data sets. DMSP shows the plasmapause at the poleward edge of the channel, whereas Cluster shows the plasmapause across the entire channel. DMSP shows a deep density trough on the equatorward side of the channel, whereas there is no indication of this in the Cluster data set. The density irregularities shown by Cluster are much smaller than the projection of the ionospheric trough. These differences highlight the complexity of MI coupling at smaller scales.

[34] The SAID generation mechanism was not discussed but rather will be saved for a future study of multiple DMSP-Cluster conjugate events. The observations presented here support the notion of active, strong MI coupling along the entire field lines in the dusk-side ring current/plasmasphere overlap region during moderate geomagnetic activity. More measurements of this type are necessary to parameterize the strength of this coupling and possibly to validate future SAPS/SAID models of the inner magnetosphere [e.g., *Goldstein et al.*, 2005a].

References

Anderson, P. C., R. A. Heelis, and W. B. Hanson (1991), The ionospheric signatures of rapid subauroral ion drifts, *J. Geophys. Res.*, *96*(A4), 5785–5792.

Anderson, P. C., W. B. Hanson, R. A. Heelis, J. D. Craven, D. N. Baker, and L. A. Frank (1993), A proposed production model of rapid subaur-

oral ion drifts and their relationship to substorm evolution, *J. Geophys. Res.*, 98(A4), 6069, 1993.

Anderson, P. C., D. L. Carpenter, K. Tsuruda, T. Mukai, and F. J. Rich (2001), Multisatellite observations of rapid subauroral ion drifts (SAID), *J. Geophys. Res.*, 106(A12), 29585.

Balogh, A., et al. (2001), The cluster magnetic field investigation: Overview of in-flight performance and initial results, *Ann. Geophys.*, 19, 1207.

Birn, J., M. F. Thomsen, J. E. Borovsky, G. D. Reeves, D. J. McComas, R. D. Belian, and M. Hesse (1997), Substorm ion injections: Geosynchronous observations and test particle orbits in three-dimensional dynamic MHD fields, *J. Geophys. Res.*, 102(A2), 2325–2342.

Burke, W., et al. (2000), Ionospheric disturbances observed by DMSP at middle to low latitudes during the magnetic storm of June 4–6, 1991, *J. Geophys. Res.*, 105(A8), 18,391.

Décréau, P. M. E., et al. (2001), Early results from the Whisper instrument on Cluster: An overview, *Ann. Geophys.*, 19, 1241–1258.

Escoubet, C. P., R. Schmidt, and M. L. Goldstein (1997), Cluster—Science and mission overview, *Space Sci. Rev.*, 79, 11.

Figueiredo, S., T. Karlsson, and G. T. Marklund (2004), Investigation of subauroral ion drifts and related field-aligned currents and ionospheric Pedersen conductivity distribution, *Ann. Geophys.*, 22, 923–934.

Foster, J. C., and W. J. Burke (2002), SAPS: A new categorization for subauroral electric fields, *Eos Trans. AGU*, 83(36), 393.

Foster, J. C., and H. B. Vo (2002), Average characteristics and activity dependence of the subauroral polarization stream, *J. Geophys. Res.*, 107(A12), 1475, doi:10.1029/2002JA009409.

Galperin, Y., Y. Ponomarev, and A. Zosimova (1974), Plasma convection in the polar ionosphere, *Ann. Geophys.*, 30, 1.

Galperin, Y., V. S. Soloviev, K. Torkar, J. C. Foster, and M. V. Veselov (1997), Predicting plasmaspheric radial density profiles, *J. Geophys. Res.*, 102(A2), 2079.

Goldstein, J., J. L. Burch, and B. R. Sandel (2005a), Magnetospheric model of subauroral polarization stream, *J. Geophys. Res.*, 110, A09222, doi:10.1029/2005JA011135.

Goldstein, J., J. L. Burch, B. R. Sandel, S. B. Mende, P. C:son Brandt, and M. R. Hairston (2005b), Coupled response of the inner magnetosphere and ionosphere on 17 April 2002, *J. Geophys. Res.*, 110, A03205, doi.10.1029/2004JA010712.

Gustafsson, G., et al. (1997), The electric field and wave experiment for the Cluster mission, *Space Sci. Rev.*, 79, 137.

Horwitz, J. L., R. H. Comfort, and C. R. Chappell (1990), A statistical characterization of plasmasphere structure and boundary locations, *J. Geophys. Res.*, 95, 7937.

Iijima, T., and T. A. Potemra (1976), The amplitude distribution of field-aligned currents at northern high latitudes observed by Triad, *J. Geophys. Res.*, 81(13), 2165.

Iijima, T., T. A. Potemra, and L. Z. Zanetti (1990), Large-scale characteristics of magnetospheric equatorial currents, *J. Geophys. Res.*, 95(A2), 991–999.

Jorgensen, A. M., H. E. Spence, W. J. Hughes, and H. J. Singer (2004), A statistical study of the global structure of the ring current, *J. Geophys. Res.*, 109, A12204, doi:10.1029/2003JA010090.

Karlsson, T., G. Marklund, L. Blomberg, and A. Mälkki (1998), Subauroral electric fields observed by Freja satellite: A statistical study, *J. Geophys. Res.*, 103, 4327.

Kistler, L. M., F. M. Ipavich, D. C. Hamilton, G. Gloeckler, B. Wilken, G. Kremser, and W. Stüdemann (1989), Energy spectra of the major ion species in the ring current during geomagnetic storms, *J. Geophys. Res.*, 94, 3579.

Laakso, H., and A. Pedersen (1998), Ambient electron density derived from differential potential measurements, in *Measurement Techniques in Space Plasmas*, edited by J. Borovsky, R. Pfaff, and D. Young, AGU Monograph 102, AGU, Washington, D. C., pp. 49–54.

LaBelle, J., R. Treumann, W. Baumjohann, G. Haerendel, N. Sckopke, G. Paschmann, and H. Lühr (1988), The duskside plasmapause/ring current interface: Convection and plasma wave observations, *J. Geophys. Res.*, 93, 2573.

Li, X., D. N. Baker, M. Temerin, G. D. Reeves, and R. D. Belian (1998), Simulation of dispersionless injections and drift echoes of energetic electrons associated with substorms, *Geophys. Res. Lett.*, 25(20), 3763–3766.

Liemohn, M. W., J. U. Kozyra, C. R. Clauer, and A. J. Ridley (2001), Computational analysis of the near-Earth magnetospheric current system during two-phase decay storms, *J. Geophys. Res.*, 106(A12), 29,531–29,542.

Maynard, N. C., T. L. Aggson, and J. P. Heppner (1980), Magnetospheric observation of large subauroral electric fields, *Geophys. Res. Lett.*, 7, 881.

Mishin, E. V., and W. J. Burke (2005), Stormtime coupling of the ring current, plasmasphere and topside ionosphere: Electromagnetic and plasma disturbances, *J. Geophys. Res.*, 110, A07209, doi:10.1029/2005JA011021.

Mishin, E. V., W. J. Burke, C. Y. Huang, and F. J. Rich (2003), Electromagnetic wave structures within subauroral polarization streams, *J. Geophys. Res.*, 108(A8), 1309, doi:10.1029/2002JA009793.

Mishin, E. V., W. J. Burke, and A. A. Viggiano (2004), Stormtime subauroral density troughs: Ion-molecule kinetics effects, *J. Geophys. Res.*, 109, A10301, doi:10.1029/2004JA010438.

Ober, D. M., J. L. Horwitz, and D. L. Gallagher (1997), Formation of density troughs embedded in the outer plasmasphere by subauroral ion drift events, *J. Geophys. Res.*, 102(A7), 14,595–14,602.

Oberhardt, M. R., D. A. Hardy, W. E. Slutter, J. O. McGarity, D. J. Sperry, A. W. Everest, A. C. Huber, J. A. Pantazis, and M. Pl Gough (1994), The shuttle potential and return electron experiment (SPREE), *IL Nuovo Cimento*, 17, 67.

Paschmann, G., et al. (1997), The electron drift instrument for Cluster, *Space Sci. Rev.*, 79, 233.

Rème, H., et al. (2001), First multispacecraft ion measurements in and near the Earth's magnetosphere with the identical Cluster ion spectrometry (CIS) experiment, *Ann. Geophys.*, 19, 1303–1354.

Rich, F. J., and M. Hairston (1994), Large-scale convection patterns observed by DMSP, *J. Geophys. Res.*, 79, 3827.

Rich, F. J., W. J. Burke, M. C. Kelley, and M. Smiddy (1980), Observations of field-aligned currents in association with strong convection electric fields at subauroral latitudes, *J. Geophys. Res.*, 85(A5), 2335.

Smiddy, M., M. C. Kelley, W. Burke, R. Rich, R. Sagalyn, B. Shuman, R. Hays, and S. Lai (1977), Intense poleward directed electric fields near the ionospheric projection of the plasmapause, *Geophys. Res. Lett.*, 4, 543.

Spiro, R., R. Heelis, and W. Hanson (1979), Rapid subauroral ion drifts observed by Atmospheric Explorer C, *Geophys. Res. Lett.*, 6, 657.

Thomsen, M., J. Birn, J. Borovsky, K. Morzinski, D. McComas, and G. Reeves (2001), Two-satellite observations of substorm injections at geosynchronous orbit, *J. Geophys. Res.*, 106, 8405–8416.

Toivanen, P. K., H. E. J. Koskinen, and T. I. Pulkkinen (1998), Mapping between the ionospheric and the tail electric fields in a time-dependent Earth's magnetosphere, *J. Geophys. Res.*, 103, 9153.

Tsyganenko, N. A. (2002a), A model of the near magnetosphere with a dawn-dusk asymmetry: 1. Mathematical structure, *J. Geophys. Res.*, 107(A8), 1179(A8), doi:10.1029/2001JA000219.

Tsyganenko, N. A. (2002b), A model of the near magnetosphere with a dawn-dusk asymmetry: 2. Parameterization and fitting to observations, *J. Geophys. Res.*, 107(A8), 1176, doi:10.1029/2001JA000220.

Valchuck, T. E., Y. I. Galperin, L. M. Nikolaenko, Y. I. Feldstein, J.-M. Bosqued, J. A. Sauvud, and J. Crasnier (1986), Equatorial border of the auroral electron diffuse precipitation zone in the morning sector (in Russian), *Kosm. Issled.*, 24, 875–883.

Vallat, C., I. Dandouras, M. Dunlop, A. Balogh, E. Lucek, G. K. Parks, M. Wilber, E. C. Roelof, G. Chanteur, and H. Rème (2005), First current density measurements in the ring current region using simultaneous multi-spacecraft CLUSTER-FGM data, *Ann. Geophys.*, 23, 1849–1865.

Vasyliunas, V. M. (1970), Mathematical models of magnetospheric convection and its coupling to the ionosphere, in *Particles and Fields in the Magnetosphere*, edited by B. M. McCormac, p. 60, Springer, New York.

Weimer, D., C. Goertz, D. Gurnett, N. Maynard, and J. Burch (1985), Auroral zone electric fields from DE1 and 2 at magnetic conjunctions, *J. Geophys. Res.*, 90, 7479.

Yeh, H.-C., J. C. Foster, F. J. Rick, and W. Swider (1991), Storm time electric field penetration observed at mid-latitude, *J. Geophys. Res.*, 96(A4), 5707.

————————

P. M. E. Décréau, LPCE/CNRS, Université d'Orléans, Orléans, France.

Y. Khotyaintsev, Swedish Institute of Space Physics, Uppsala, Sweden.

L. Kistler, H. Matsui, C. Mouikis, and P. A. Puhl-Quinn, Space Science Center, University of New Hampshire, 39 College Road, Durham, NH 03824, USA. (pamela.puhlquinn@unh.edu)

E. Lucek, Blackett Laboratory, Imperial College, London, UK.

E. Mishin, Institute for Scientific Research, Boston College, Chestnut Hill, MA, USA.